

# CHARGE STORAGE, CONDUCTIVITY AND CHARGE PROFILES OF INSULATORS AS RELATED TO SPACECRAFT CHARGING

**J.R. Dennison**

Physics Department, Utah State University  
Logan, UT, USA 84322-4415  
Phone: (435) 797-2936  
Fax: (435) 797-2492  
E-mail: [JR.Dennison@usu.edu](mailto:JR.Dennison@usu.edu)

**Prasanna Swaminathan**

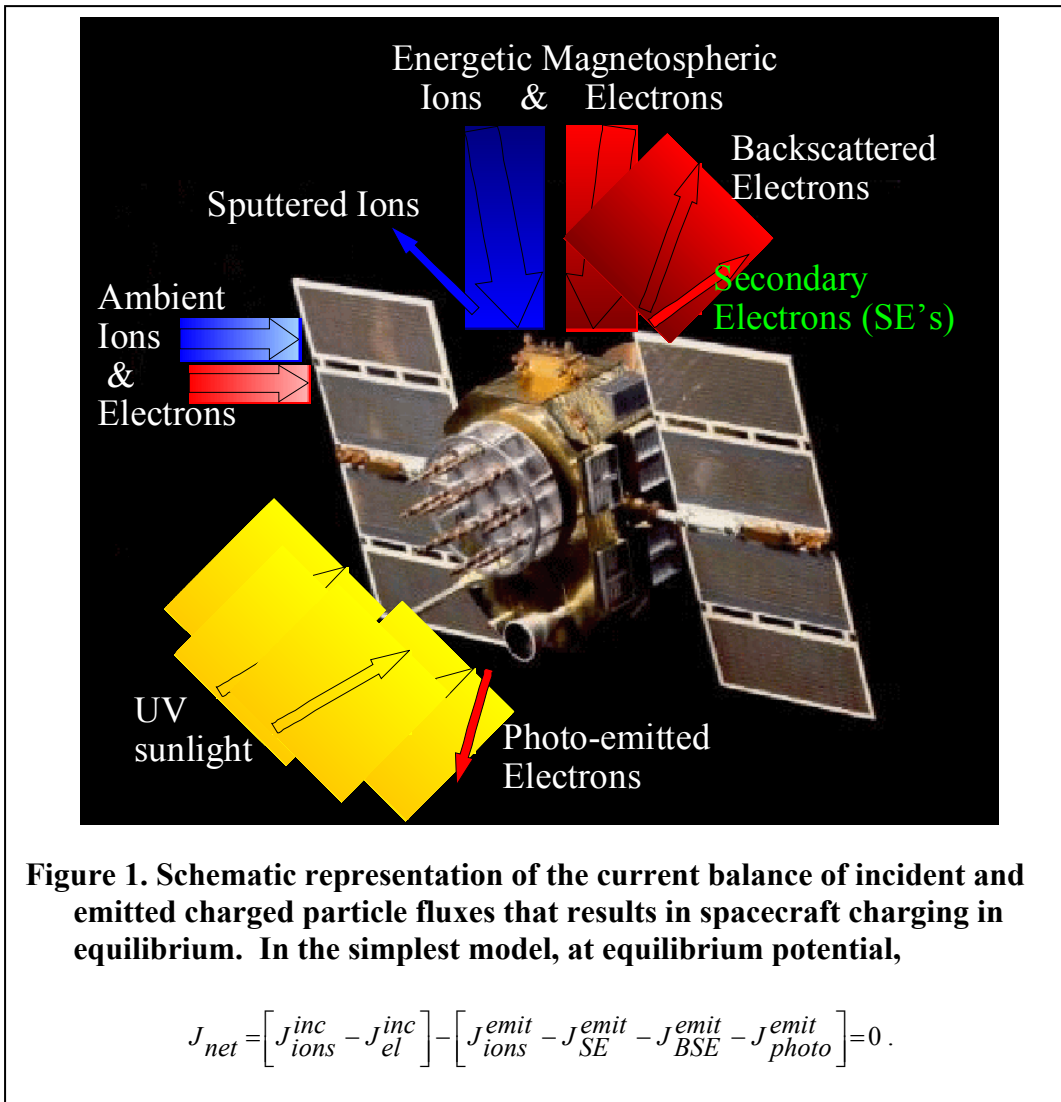
Physics Department, Utah State University

**A. R. Frederickson**

Caltech Jet Propulsion Laboratory

## Abstract

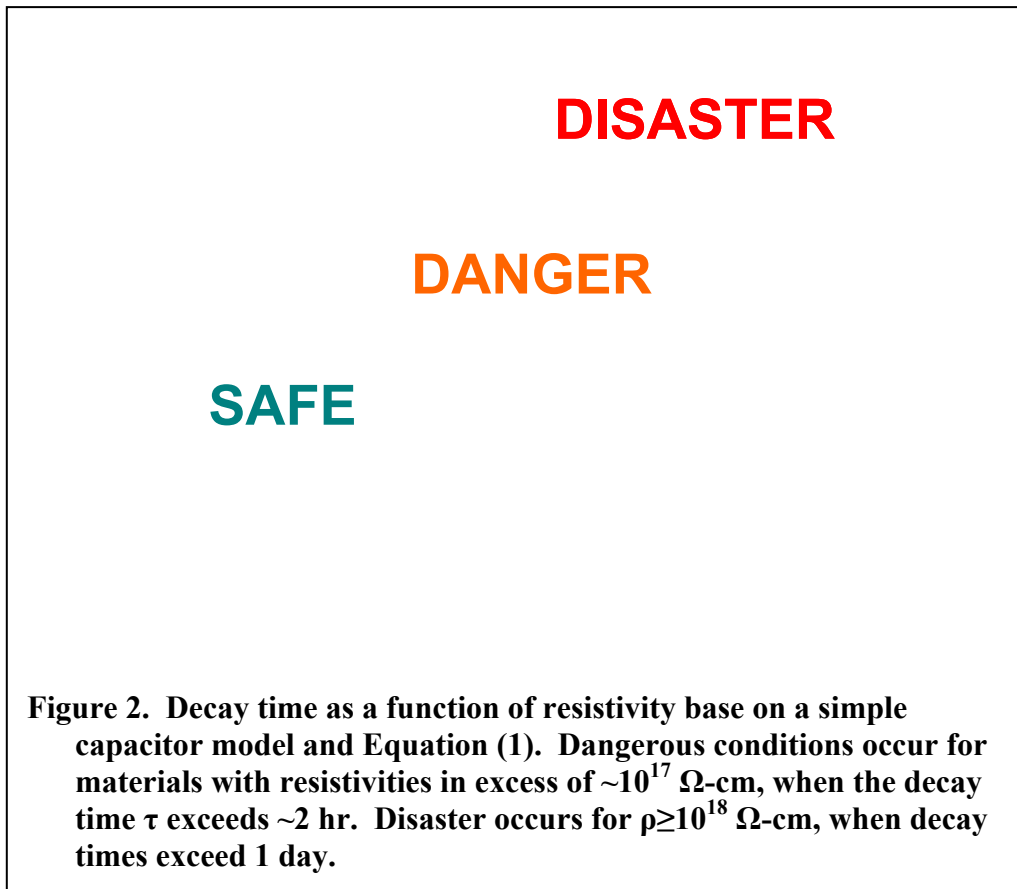
Dissipation of charges built up near the surface of insulators due to space environment interaction is central to understanding spacecraft charging. Conductivity of insulating materials is key to determine how accumulated charge will distribute across the spacecraft and how rapidly charge imbalance will dissipate. To understand these processes requires knowledge of how charge is deposited within the insulator, the mechanisms for charge trapping and charge transport within the insulator, and how the profile of trapped charge affects the transport and emission of charges from insulators. One must consider generation of mobile electrons and holes, their trapping, thermal de-trapping, mobility and recombination. Conductivity is more appropriately measured for spacecraft charging applications as the "decay" of charge deposited on the surface of an insulator, rather than by flow of current across two electrodes around the sample. We have found that conductivity determined from charge storage decay methods is  $10^2$  to  $10^4$  smaller than values obtained from classical ASTM and IEC methods for a variety of thin film insulating samples. For typical spacecraft charging conditions, classical conductivity predicts decay times on the order of minutes to hours (less than typical orbit periods); however, the higher charge storage conductivities predict decay times on the order of weeks to months leading to accumulation of charge with subsequent orbits. We found experimental evidence that penetration profiles of radiation and light are exceedingly important, and that internal electric fields due to charge profiles and high-field conduction by trapped electrons must be considered for space applications. We have also studied whether the decay constants depend on incident voltage and flux or on internal charge distributions and electric fields; light-activated discharge of surface charge to distinguish among differing charge trapping centers; and radiation-induced conductivity. Our experiments also show that "Malter" electron emission occurs for hours after turning off the electron beam. This Malter emission—similar to emission due to negative electron affinity in semiconductors—is a result of the prior radiation or optical excitations of valence electrons and their slow drift among traps towards the surface where they are subsequently emitted. This work is supported through funding from the NASA Space Environments and Effects Program.



### Introduction

In the space environment, charge is deposited on the surface of the spacecraft as it orbits. Hence, the orbital periodicity sets the relevant time scale for the problem; typical orbits of near-earth satellites range from 1 to 24 hours. For example, satellite orbit or rotation period determines the time surfaces are exposed to sunlight and subject to photoemission. Charge accumulated on the insulating spacecraft surfaces typically dissipates through the insulator to a conducting substrate. To better understand the charging phenomena, one then needs to relate conductivity or charge mobility to a suitable time scale. The charge storage decay time to the conducting substrate depends on the (macroscopic) conductivity or equivalently the (microscopic) charge mobility for the insulator. If the charge decay time exceeds the orbit time, not all charge will be dissipated before orbital conditions again charge the satellite, and charge can accumulate. As the insulator accumulates charge, the electric field rises until the insulator breaks down and generates a pulse.

In the simplest model of spacecraft charging, the charge on satellite surfaces accumulates in such a way as to produce an electric field that modifies the incident and emitted charge particle fluxes so that a net current balance and charge equilibrium is achieved. This current balance is depicted in Figure 1. The model is plausible, if simplistic, for a fully conductive spacecraft for which the charge will readily redistribute over the entire satellite in the case of absolute charging (or over isolated sections, for differential charging). The surface of conductors will charge to the point where the incident currents from the environment fluxes are equal to emission currents. By contrast, as insulating spacecraft materials accumulate charge, their low charge mobility causes



charge to accumulate where deposited, and the local electric fields to rise until the leakage current from the insulators to underlying conductors equals the accumulation current from the environment (or until the charge stored in the insulator actually breaks down and generates a charge pulse). Hence, conductivity of insulating materials is a key transport parameter to determine how accumulated charge will distribute across the spacecraft, how rapidly charge imbalance will dissipate, and what equilibrium potential an insulator will adopt under given environmental conditions [1].

Treating a thin film insulator as simple capacitor, charge decay time is proportional to resistivity. As a first approximation, the thin-film insulator can be treated as a planar capacitor (with the charged front surface and conducting rear electrode acting as the electrodes); all charge resides at the interfaces, that discharges in an Ohmic fashion through the bulk of the insulator. In

this approximation, the RC-time constant or relaxation time,  $\tau$ , for discharging insulator can be written as:

$$\tau = \rho \epsilon_r \epsilon_0 \quad (1)$$

where  $\rho$  is the material resistivity, and  $\epsilon_0$  is the permittivity of free space. The relative dielectric constant,  $\epsilon_r$ , of nearly all spacecraft insulators lie within a narrow range, 2-10, and is well known for most materials; thus, determination of the resistivity follows directly from measuring the relaxation time. The decaying surface potential can then be estimated as a function of time as  $\sigma(t) = \sigma_0 \cdot e^{-t/\tau}$ , where  $\sigma_0$  is the initial sample surface charge induced by electron beam irradiation, and  $\sigma$  is the decayed surface charge after a time interval,  $t$ . Therefore,  $\tau$  is equivalently the relaxation time or the charge storage decay time, the time it takes for the surface charge to drop to  $1/e$  of its initial value. Note that in this simple model, decay time is an intrinsic material property, independent of surface area or thickness.

Figure 2 shows a plot of decay time as a function of resistivity, Equation (1), for a relevant range of resistivity values. Values of typical spacecraft insulator material resistivities found in handbooks are in the range of  $10^{13}$  to  $10^{17}$   $\Omega$ -cm [2]. These corresponding to decay times of  $\sim 1$  sec to  $\sim 2$  hr, suggesting that in most cases charge collected by common spacecraft insulators will dissipate faster than the charge is renewed. Considering these results, dangerous conditions occur for materials with resistivities in excess of  $\sim 10^{17}$   $\Omega$ -cm, when  $\tau$  exceeds  $\sim 2$  hr. Disastrous conditions occur for  $\rho \geq 10^{18}$   $\Omega$ -cm, when decay times exceed 1 day.

Thus, it becomes critical for reliable spacecraft charging modeling to determine appropriate values of resistivity for typical thin film insulating materials [1,3,4]. The bulk resistivity values of insulators used to model spacecraft charging have traditionally been obtained from the handbook [2] values found by the classical ASTM/IEC methods [5,6]. However, recent work has shown that these classical methods are often not applicable to situations encountered in spacecraft charging [1,3,4,7,8]. The charge storage method—described below—was developed to measure the resistivity in a more applicable configuration. Results from charge storage resistivity methods find  $\rho$  values  $10^1$ - $10^4$  times larger than classical handbook values, based on tests performed by Frederickson and coworkers on approximately ten different materials, including polyimides, Mylar<sup>TM</sup>, Teflon<sup>TM</sup>, silicate glasses, and circuit boards [1,3,4]. Returning to Figure 2, the relevant decay times corresponding to the higher charge storage resistivities of

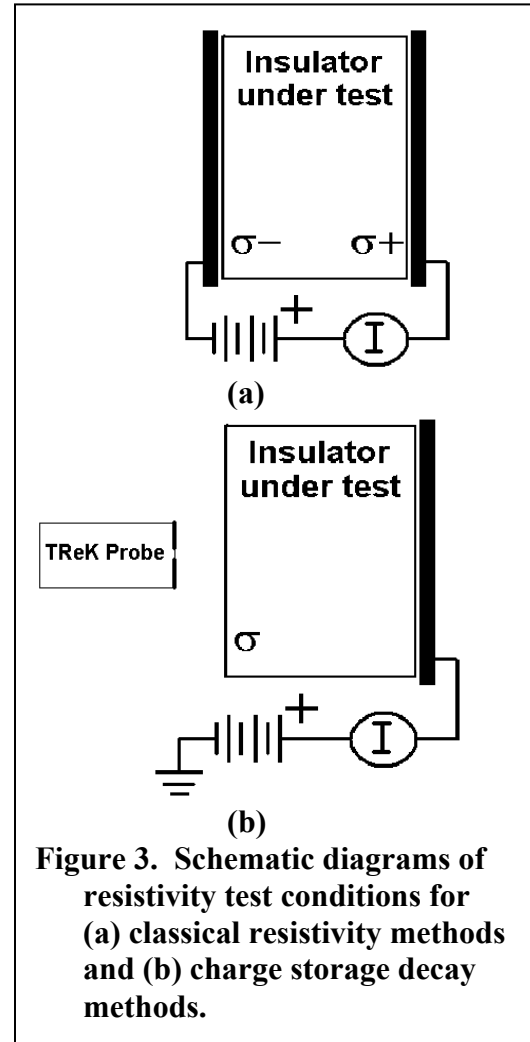


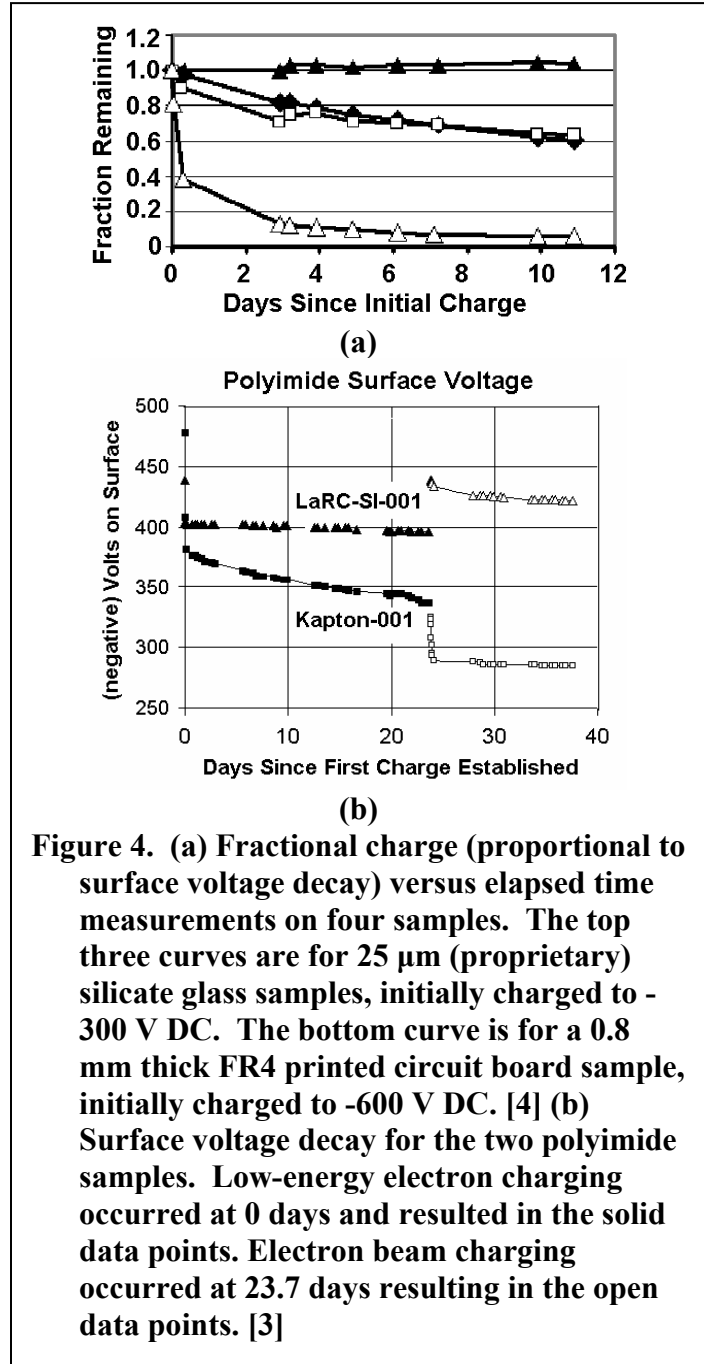
**Figure 3. Schematic diagrams of resistivity test conditions for (a) classical resistivity methods and (b) charge storage decay methods.**

these typical spacecraft insulators in the range of  $10^{14}$  to  $10^{21}$   $\Omega\cdot\text{cm}$  are  $\sim 1$  min to several years, clearly in the danger or disaster zones. Resistivity values based on the charge storage method have recently been used to correctly predict charging events observed in real satellite data, through modeling of pulses occurring aboard the CRESS satellite (see below) [8]. Given these results, we have concluded that charge storage resistivity methods are more appropriate than classical methods for many spacecraft charging problems.

This paper describes measurements of the decay of charge deposited on the surface of insulators or within a narrow region below the surface. The work is a joint project by the Jet Propulsion Laboratory (JPL) and Utah State University (USU) sponsored through the NASA Space Environments and Effects (SEE) Program [7]. All data presented in this paper were taken at JPL. Preliminary studies using the charge storage method and further details of the methods and instrumentation are found elsewhere [1,3,4]. Swaminathan, *et al.* provides a detailed comparison between classical and charge storage methods used to measure resistivity [1].

### Comparison of Resistivity Test Methods

Classical methods use a parallel plate capacitor configuration to determine the conductivity of insulators by application of a constant voltage ( $E$ -field) and the measurement of the resulting leakage current across the plates and through the insulator [1,5,6]. Figure 3(a) shows the preferred experimental arrangement for the ASTM-IEC or classical resistance method that is valid in the range of  $10^7 < \rho < 10^{21}$   $\Omega\cdot\text{cm}$  [6,7]. An adjustable high voltage is applied to one sample electrode. Current flow to the sample electrode held at ground is measured by a picoammeter. The resistance of the sample is then given by  $R = \rho d / A_{eff}$ , where  $\rho$  is the resistivity,  $A_{eff}$  is the effective area slightly larger than the metal electrode surface area, and  $d$  is the sample thickness. The resistance  $R$  is determined from an I-V curve using Ohm's law.



Data obtained using the classical resistance method for specific spacecraft materials such as Kapton H [9] and FR4 printed circuit board [4] materials are provided in other references [1,3,4]. Comparisons between classical and charge storage decay methods for some specific samples are made below; other such results are given in Refs. 1 and 4.

The voltages developed in space are usually generated by impressing charge into the insulation, not by the application of voltage from a power supply onto electrodes. Conductivity is more appropriately measured for spacecraft charging applications as the "decay" of charge deposited on the surface of an insulator. The arrangement for charging and measuring the surface charge (or voltage) on an insulated surface is shown in Figure 3(b). Charge decay methods expose one side of the insulator in vacuum to a charge source for deposition and treatments or to a field probe for charge monitoring. The other surface of the sample is in good contact with a conducting electrode and is connected to wiring so that it can be biased relative to ground or electron source, and can be monitored for currents. A TReK™ electrostatic voltmeter [10] is used, that can sense surface voltages from -20 kV to +20 kV relative to local "ground," and from this infer local surface charge distributions. No electrical contact is made to the nearby HV surface. A custom capacitance transfer probe was constructed at JPL to make electric field measurements at sample surfaces *in situ* in a vacuum chamber, using a TreK™ probe external to the chamber; this isolates the sensitive TreK™ probe from the charge sources and sample treatments.

A variety of charged particle sources for deposition and sample treatment are available. For the basic charge storage measurements, a low energy (<10 eV) electron-emitting filament is used to provide uniform surface charge that does not penetrate far into the sample. This method (described in detail in Ref. 1) places the electrons gently onto the front surface, not deeper into the bulk of the insulator. Alternately, a broad-beam electron gun with accelerating potentials from 0 to 75 keV is available for uniform, stable charge deposition at energies in the few keV regime near the second crossover energy and at higher energies for study of internal sample charging. In addition, samples can be pre-treated using, low-energy electron fluxes, the higher energy electron beam, VIS/UV light photon fluxes, plasma sources, ion fluxes, and thermal treatments.

**Table 1. Resistivity Models for CRRES Data from FR4 Printed Circuit Board Samples.**

<b>Method Used to Determine Resistivity</b>	<b>Dark Resistivity (Ω-cm)</b>	<b>Radiation-Induced Resistivity (Ω-cm)</b>	<b>Total Resistivity (Ω-cm)</b>	<b>Relaxation Time (hr)</b>
Classical Method	$5 \times 10^{17}$	$3 \times 10^{18}$	$2 \times 10^{17}$	5
Charge Storage Method	$2 \times 10^{18}$	same	$1 \times 10^{18}$	31
Best Fit to Pulse Data	$6 \times 10^{18}$	same	$2 \times 10^{18}$	52

Figures 4(a) [4] and 4(b) [3] show charge storage decay curves for six different materials. In each case, the resistivity is two to four orders of magnitude larger than that obtained with classical methods. For example, the charge storage value of resistivity for aluminum-backed 51 μm Kapton H samples [4] was  $>5 \cdot 10^{+19}$  Ω·cm [see Fig. 4(b)], compared to a value of  $\sim(3 \pm 1)$

$\cdot 10^{+16} \Omega\cdot\text{cm}$  measured with classical methods and a handbook value of  $1 \cdot 10^{+17} \Omega\cdot\text{cm}$  [9]. Note that charge decay is measured on timescales reasonably similar to that experienced in space, at least a month, to correctly evaluate appropriate decay.

### Application of Charge Storage Resistivity to Charging Modeling

Frederickson and Brautigam have recently completed a study [8] of Internal Discharge Monitor (IDM) pulse data [11] from sample aboard the *Combined Release and Radiation Effects Satellite* (CRRES) [12], which provides compelling evidence for the validity of using charge storage resistivity values in spacecraft charging modeling. The project used only basic laboratory-derived materials properties (including resistivity) and data from on-board environmental charge flux monitors as inputs to models for internal charge deposition and migration within test samples to successfully predict the sample electrostatic discharge (ESD) pulsing amplitude and frequency over a time scale of hundreds of days and more than a thousand orbits. Central to the success of the project was the use of the charge storage resistivity in place of the classical value of resistivity.

Specifically, data records were mined for IDM pulse data as a function of elapsed time for a variety of insulator samples, including a 0.8 mm thick FR4 printed circuit board sample, shown in the middle graph of Figure 5. Concurrent electron environmental data over a range of energies from  $\sim 0.1$  to 5 MeV were also mined and parameterized to obtain a dosage profile impinging on the sample as a function of elapsed time over the  $\sim 15$  month lifetime of the satellite. These parameterized dosage profiles for each half-orbit ( $\sim 5$  hr period) were used, together with stopping power and conductivity data for the sample materials, to model the charge deposition profile, the

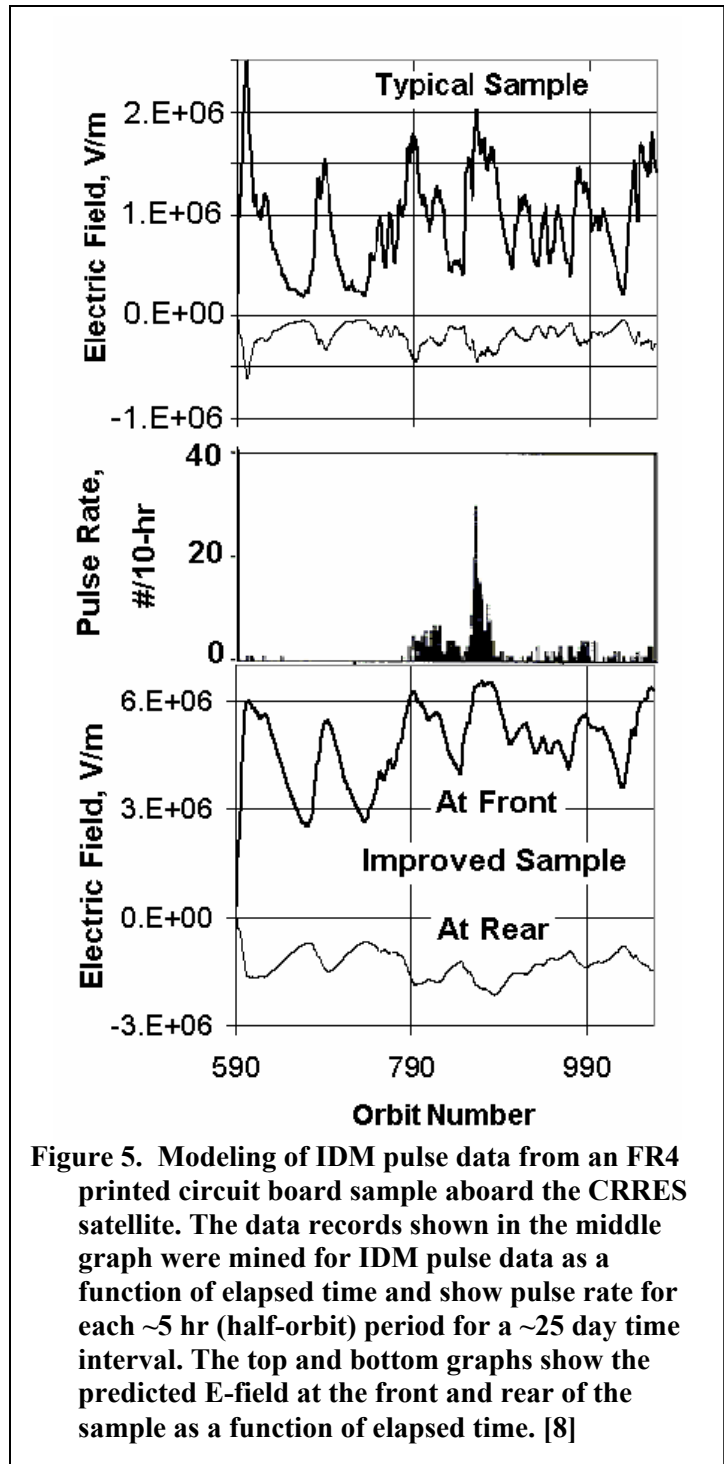


Figure 5. Modeling of IDM pulse data from an FR4 printed circuit board sample aboard the CRRES satellite. The data records shown in the middle graph were mined for IDM pulse data as a function of elapsed time and show pulse rate for each  $\sim 5$  hr (half-orbit) period for a  $\sim 25$  day time interval. The top and bottom graphs show the predicted E-field at the front and rear of the sample as a function of elapsed time. [8]

charge transport, and the time evolution of the internal charge distribution. The NUMIT code [13] was then used to calculate and time-evolving E-field profile.

The top and bottom graphs in Figure 5 show the predicted E-field at the front and rear of the sample as a function of elapsed time. The top panel is based on the classical resistivity value of FR4 board and an estimated value of the radiation-induced conductivity based on results for similar materials (values are listed in Table I). Note that at no time does the E-field in the top panel of Figure 5 exceed 25% of the value of  $1 \cdot 10^7$  V/m, which is typically needed to induce occasional pulsing. This prediction of no pulsing is consistent with the observation that the relaxation time from the total resistivity (dark resistivity and radiation-induced resistivities added in parallel) based on Equation (1) of  $\sim 5$  hr is less than the orbit time of  $\sim 10$  hr. However, when the measured charge storage resistivity is used to predict the E-field evolution (see lower panel of Figure 5), the E-field exceeds  $0.6 \cdot 10^7$  V/m near 600, 790, 850 and 1050 orbit number. In each case, there is corresponding pulse activity observed in the central panel of Figure 5, with the pulse rate amplitude correlated to the magnitude of the E-field. Again, the prediction of pulsing is consistent with the predicted relaxation time of  $\sim 31$  hrs from Equation (1), which is well in excess of the orbit time. Finally, a value of dark resistivity that best fits the pulse data was determined. Note that because the charge storage resistivity and the estimated radiation-induced resistivity are comparable, the total resistivity of the best fit is only a factor of two larger than the total resistivity using the measured charge storage resistivity.

### Effects of Internal Charge Distributions

Given the preliminary results from charge storage measurements of spacecraft insulators and the successful use of these measurements to model charge storage and dissipation and to predict pulsing in real world applications, it is tempting to consider the problem solved and simply use charge storage resistivities in place of classical resistivities for future modeling. However, the question of why the classical and charge storage methods produce resistivity values that differ by as much as four orders of magnitude still needs to be addressed, if for no other reason than to know which resistivity value to use for different circumstances (to say nothing of understanding the questions of the underlying physics).

While there is yet no clear explanation as to why the two methods produce such divergent results,

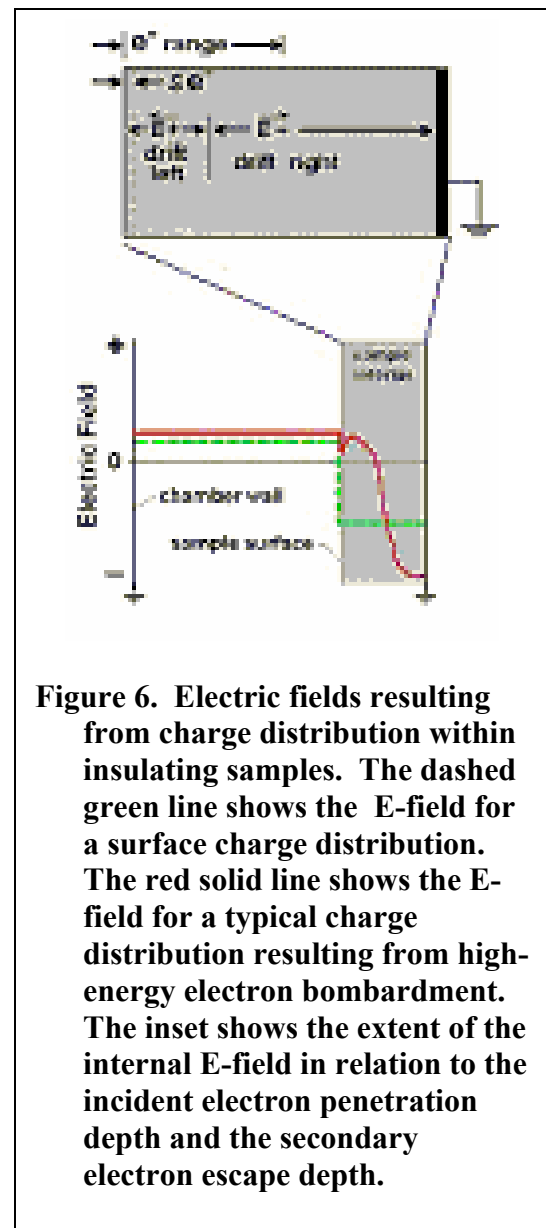


**Figure 6. Electric fields resulting from charge distribution within insulating samples. The dashed green line shows the E-field for a surface charge distribution. The red solid line shows the E-field for a typical charge distribution resulting from high-energy electron bombardment. The inset shows the extent of the internal E-field in relation to the incident electron penetration depth and the secondary electron escape depth.**



preliminary results suggest internal charge distribution and electric fields are critical to understanding the underlying physics. To illustrate these processes requires knowledge of how charge is deposited within the insulator, the mechanisms for charge trapping and charge transport within the insulator, and how the profile of trapped charge affects the transport and emission of charges from insulators. One must consider generation of mobile electrons and holes, their trapping, thermal de-trapping, tunneling, mobility, recombination and emission from the sample.

A number of experiments have been conducted in this project to investigate the role of charge deposition, charge transport and charge decay in materials properties such as conductivity and electron emission. In general, these experiments involve determining the effects of different sources and sample treatments, such as high-energy electron beams and radiation sources, ion sources, plasma sources, visible and UV light treatments, thermal treatments, or other treatments of the samples [4]. To evaluate conduction in unaltered insulators, their surfaces must be charged with low-energy electrons, as described above. Kilovolt electron beams, ions, or other treatments alter the sample as they excite secondary processes that repopulate trapping states in the insulator, or otherwise alter the material.

### **Charge deposition and distribution**

We begin by describing where charge is deposited in an insulator and how this is affected by the incident particle energy and the charge distribution already present in the insulator. Consider the electric fields resulting from charge distributions in the insulator depicted for a 1D scenario schematically in Figure 6. For very low incident energies, the mean free path of the incident electrons is very small (on the order of nanometers) and, to a good approximation, charge is deposited on the insulator surface. Such a surface charge distribution is also appropriate for a biased conducting surface [14] where charge produced in the interior rapidly migrates to the surface. A charge distribution confined to the surface results in a uniform  $\mathbf{E}$ -field everywhere within the ideal insulator between the charged surface and the grounded rear electrode. The field is also constant external to the charged surface between a parallel grounded plate and the charge plane. The magnitude of the external field is typically much less than the internal field, as the ratio of the  $\mathbf{E}$ -fields scales with the inverse ratio of the distances from the charged surface and the grounded planes. The surface charge on an insulator presents a barrier to incident electrons in the same manner as for a biased conductor [14]. Those incident electrons with insufficient energy to overcome the surface potential barrier are turned away; those with higher energies have their landing energies reduced.

Higher energy electrons penetrate further into the surface; for kilovolt electrons this can be on the order of  $\mu\text{m}$  for insulators. Because space radiation injects charge into the interior of the insulator, generally the highest voltage is achieved internal to the insulator. A simple approximation is that all charge is deposited in a plane at a uniform depth, equal to the mean free path of the incident electrons. Note that this approximation is that used for the stopping power in the Sternglass formulation of the secondary electron yield formula [15]. If the plane of charge is moved into the insulator to the depth of the mean free path, the electric displacement on the left side of the charge plane remains unchanged, but the constant electric field inside the left side of the insulator is decreased by a factor of  $1/\epsilon_r$ . An alternate approximation for high-energy electron penetration is that the number of energy loss scattering events (or equivalently, the

number of SEs generated) for the incident electrons is independent of depth (or equivalently, that the stopping power is constant), up to the penetration depth where all incident electron energy has been dissipated. (Note, this approximation is used for the constant loss formulations of the secondary electron yield formula [16]. Other models for SE yield, termed power law models, assume stopping power is proportional to the incident electron energy to the  $n^{\text{th}}$  power, where  $1 < n \leq 2$ ; these reflect that higher energy electrons will produce more SE's and lead to a higher SE production near the surface [16]. ) Any of these models provide a way to model the charge distribution inside an insulator, assuming that charge is not mobile and that the subsequent deposition is not affected by the presence of an internal charge distribution.

A more reliable picture for a typical charge distribution set up by high-energy electron bombardment is substantially more complex, if we consider charge mobility and the affect of the charge distribution of subsequent deposition. An appropriate model for this is illustrated by the solid line of the main curve in Figure 6 and the accompanying inset. Negative charge is deposited in the insulator up to some range of the incident energy electrons, typically on the order of  $\mu\text{m}$ . For typical insulators, the stopping power is found to be a larger exponent than for most metals, leading to non-linear charge deposition and reflecting the effect of charge build up in the insulator on deposition [17]. Over a narrow depth below the surface—determined by the mean free path of low-energy SEs, which are most commonly on the order of a few eV—the number of secondary electron that leave the sample often exceeds the number of electrons deposited by the incident beam; this leads to a net positive charge distribution in the SE electron region indicated in Figure 6. Thus, there can be a charge double-layer at the surface. That is, there is a sample region near the surface with an  $\mathbf{E}$ -field to the left, a sample region on the right with an  $\mathbf{E}$ -field to the right, and a zero-field plane between these two regions. The zero-field plane is typically found between the incident electron penetration depth and the SE escape depth and is the depth where the voltage is most negative [22]. The depth of the zero-field plane will increase with increasing penetration depth or incident beam energy.

Figure 6 illustrates a specific situation where the thickness of the sample is about 1/3 of the distance to the vacuum wall, and therefore the electric field in the vacuum region is roughly 1/3 of that in the sample assuming surface charge only. In real spacecraft arrangements, the distance to ground in the vacuum is very much greater than the sample thickness. Thus, in real spacecraft, the electric field strength in the back of the insulator is perhaps a hundred times larger than that in the front. Figure 6 also illustrates incident electrons with a penetration depth about  $\frac{2}{3}$  of the sample thickness. As incident electron energy increases, the incident electron range increases and the maximum voltage at the zero-field plane approaches the grounded rear electrode, resulting in an increased electric field strength.

## Charge migration

We next look at how the internal charge distribution can affect the migration of charge (conductivity). Figure 7 shows a qualitative picture of the simplified band level diagrams of an insulating sample exposed to successively higher fluxes of high-energy electron irradiation, beginning with a virgin sample in Figure 7(a). As high-energy electrons enter the insulator, they deposit energy in the region up to the penetration depth, which excites electrons into the conduction band [see Figure 7(b) and (c)]. There is typically one electron-hole pair generated for

each  $\sim 30$  eV (that is  $\sim 3 E_{\text{gap}}$ ) lost by the incident electron, and perhaps 40 such electron-hole pairs can be generated for each kilovolt of incident electron energy dissipated. As charge builds up within the insulator, the maximum voltage at zero-field plane increases, resulting in the band-bending behavior illustrated in Figures 7(b) and (c).

Electrons in the region to the left of the zero-field plane are driven to the left. The conductivity of an insulator is altered as radiation-induced excited electrons accumulate and trapped states are filled with electrons. Thermal emission from shallow traps to the conduction band occurs (slowly) everywhere that shallow traps are occupied. This is typically a small effect at room temperature. The conduction electrons are then preferentially driven in the direction of the  $\mathbf{E}$ -field, but are quickly recaptured in another trapped state. This leads to what is referred to as hopping conductivity, as the electrons preferentially progress in short “hops” from one trapped state to the next, with a net motion in the direction of the  $\mathbf{E}$ -field. As these hopping electrons reach the surface, they can be thermally excited from a trapped state to an energy sufficient to overcome the surface potential barrier. The distance from the zero-field plane, where the voltage is maximum, through the sample surface and across the vacuum is large, and therefore the electric field in this region is relatively small.

If the interior charge build up is large enough, the peak voltage can exceed the vacuum level of the sample. This means that as hopping electrons progress towards the surface they will encounter a point at which they will be excited to a conduction band state above the vacuum level. At this point, the sample is said to have a negative electron affinity and the electrons can proceed unimpeded to the surface and across the surface barrier. This negative electron affinity effect can greatly extend the region over which SEs can escape the material, thereby dramatically increasing SE yield [18]. Because electrons involved in hopping conductivity undergo slow transitions from trapped states to the conduction band states, after the irradiation stops, thermal emission currents may persist for some time until the shallow traps have emptied. This is called the Malter Effect [19].

Trapped electron moving from the zero-field plane to the right can proceed via hopping conductivity, or by an alternate method called tunneling [see Figures 7(d), (e) and (f)]. From the zero-field plane, the distance to the sample electrode is short and therefore the electric field near the electrode is large. The field can be further enhanced by using higher energy electrons to bring the penetration depth, as well as the maximum voltage zero field plane, closer to the rear electrode of the sample. This field in the back of the sample can become so large that shallow-trapped electrons tunnel to the conduction band and provide enhanced conductivity. This can occur in a range of field strength similar to that in which electrical breakdown *easily* occurs ( $>5 \times 10^5$  V/cm), and may either contribute to breakdowns or prevent them by reducing charge build-up through increased conductivity, depending on the nature of the defects that are responsible for the breakdowns.

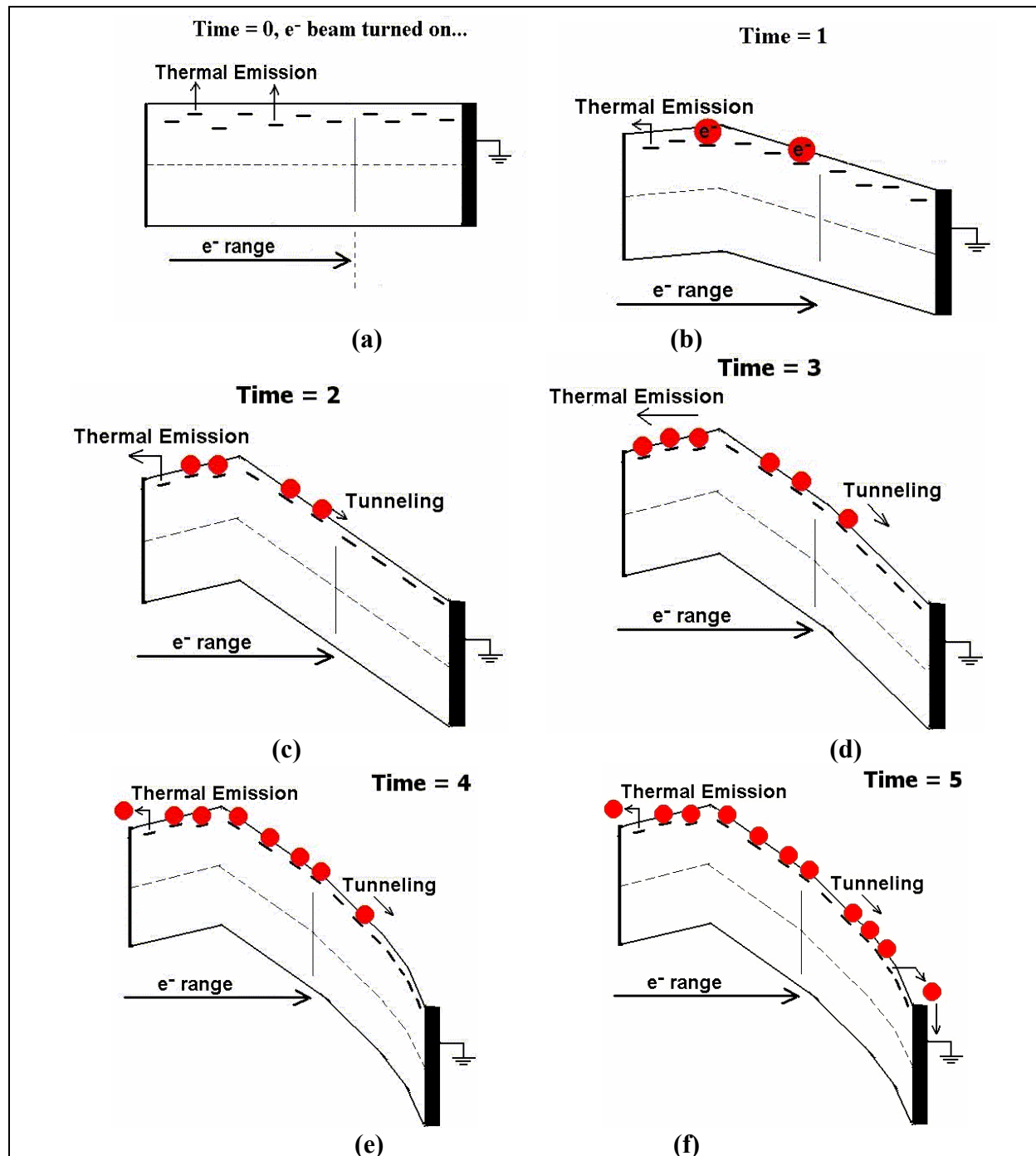
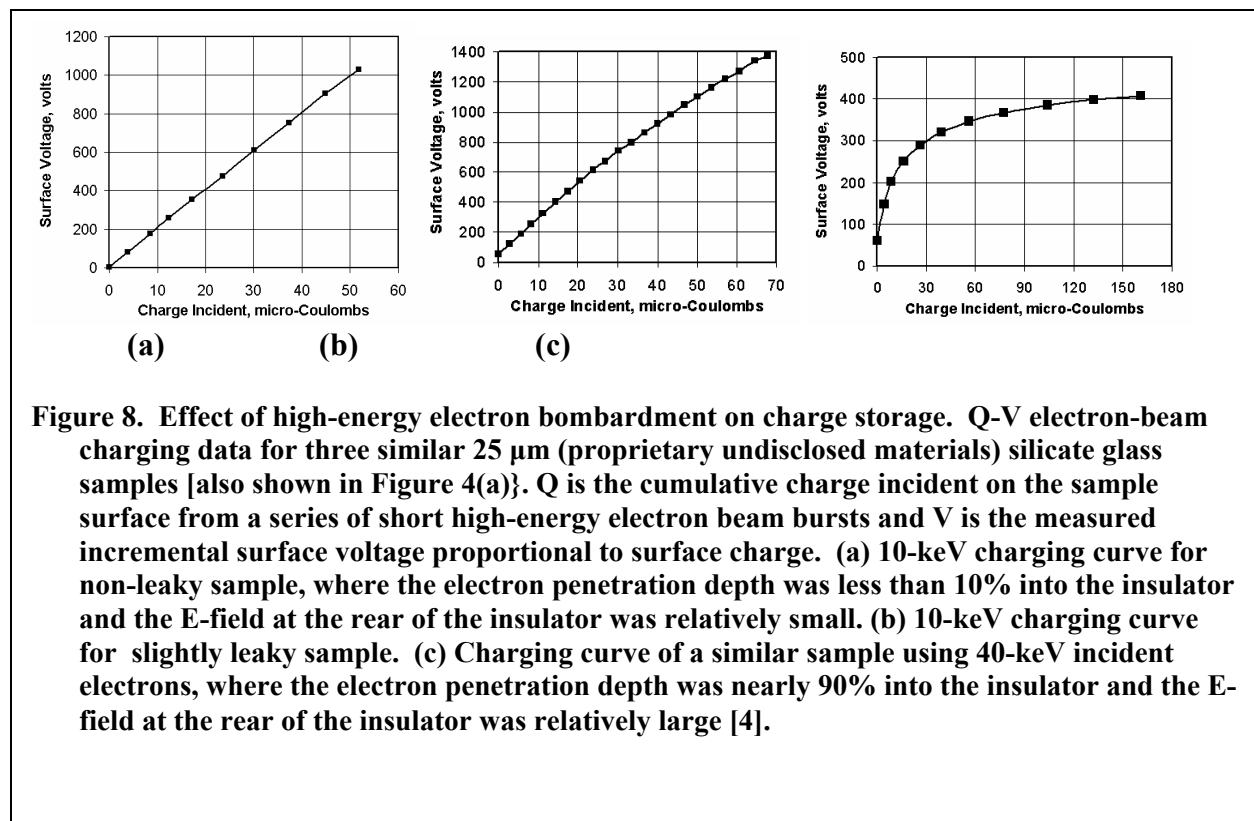


Figure 7. Simplified band diagrams for an insulating sample exposed to successively higher fluxes of high-energy electron irradiation. The horizontal axis is depth into the sample, from the charged surface on the left to the grounded rear electrode on the right. The incident electron penetration depth (typically on the order of  $\mu\text{m}$ ) shown is approximately  $\frac{2}{3}$  of the sample thickness, so that the zero-field plane where peak voltage occurs is about  $\frac{1}{3}$  of the way into the sample. The vertical axis is energy, beginning at the bottom with the valance band at  $E_{VB}$  (solid line), then the Fermi level at  $E_F$  (dashed line), localized trapped states (long dashes), and conduction band at  $E_{CB}$  (solid line). The position of the Fermi level will move towards the conduction band as the concentration of localized trapped states increases. The vacuum level,  $E_{vac}$ , is typically somewhat above  $E_{CB}$ . To set the scale, note that typical insulator band gaps,  $E_{gap} \equiv E_{CB} - E_{VB}$ , are  $\sim 5$  eV to 10 eV. The red dots represent electrons excited by the incident high-energy electrons into the conduction band, that have subsequently decayed into trapped states.

## Observed effects due to high-energy electron pre-treatments

Figures 8(a) and 8(b) shows Q-V electron-beam charging data for three similar 25  $\mu\text{m}$  silicate glass samples (proprietary, undisclosed materials) [also shown in Figure 4(a)]. Here Q is the cumulative charge incident on the sample surface from a series of short high-energy electron beam pulses and V is the measured incremental surface voltage proportional to surface charge. For Figure 8(a) [top curve in Figure 4(a)], a 10 keV electron beam was used for which the electron penetration depth was less than 10% into the insulator and the **E**-field at the rear of the insulator was relatively small. Currents arriving at the sample surface and the sample electrode were small and not affected by the developing surface voltage, as demonstrated by the straight line in Figure 8(a) for the good, non-leaky insulator. The material used for Figure 8(b) [middle curve in Figure 4(a)] was manufactured to be more conductive. The slight curvature of the trace in Fig. 8(b) indicates the occurrence of conduction currents during the time of charge-up irradiation, that is that this is a slightly leaky insulator. The insulator's capacitance was determined from the slope of the curve at small Q.

This contrasts with the behavior shown in Figure 8(c) for which, the sample behaves as a capacitor during early irradiation, whereas it behaves as a voltage regulator during continued irradiation. Figure 8(c) shows data for the same glass samples irradiated with 40 keV electrons, where the deepest incident electrons penetrate nearly 90% into the sample. In this case, the zero-field plane is much closer to the rear grounded electrode; thus, the electric field in the rear of the sample is much larger, many electrons are excited into traps near the rear electrode, and tunneling currents are larger.



**Figure 8. Effect of high-energy electron bombardment on charge storage. Q-V electron-beam charging data for three similar 25  $\mu\text{m}$  (proprietary undisclosed materials) silicate glass samples [also shown in Figure 4(a)]. Q is the cumulative charge incident on the sample surface from a series of short high-energy electron beam bursts and V is the measured incremental surface voltage proportional to surface charge. (a) 10-keV charging curve for non-leaky sample, where the electron penetration depth was less than 10% into the insulator and the **E**-field at the rear of the insulator was relatively small. (b) 10-keV charging curve for slightly leaky sample. (c) Charging curve of a similar sample using 40-keV incident electrons, where the electron penetration depth was nearly 90% into the insulator and the **E**-field at the rear of the insulator was relatively large [4].**

Figure 8(c) hints that the various radiation-generated conduction mechanisms in these glass samples prevent the development of a strong electric field, provided there is sufficient beam that penetrates throughout the sample. On these samples with 40-keV beams, much smaller surface voltage is produced than is produced with 10- or 20-keV electron beams even though at all three energies all of the electrons are stopped in the insulator. This is evidenced by the large curvature and low surface voltage in Figure 8(c), resulting from large charge bleed-off due to the enhanced conductivity. Charging induced by electron irradiation is strongly modified by the electron-hole pairs that the irradiation generates in the insulator. High field effects at or above  $10^6$  V/cm act strongly on the electron-hole pairs and on electrons in shallow traps to provide extended conductivity which can be evaluated by measuring surface voltage on the insulator. Also note that monitoring surface voltage while irradiating with electrons that stop just short of penetrating the insulator provides a way to roughly evaluate electron mean free path in an insulating material.

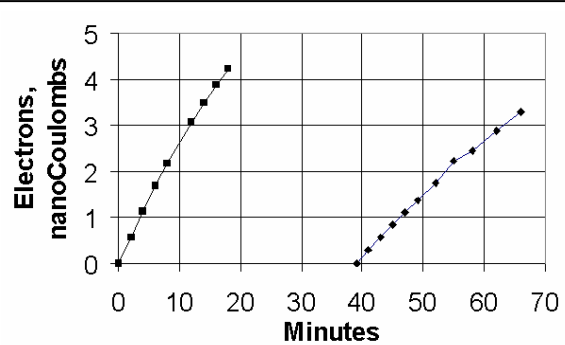


**Figure 9. Electron emission into the vacuum after irradiation ceases. The 25  $\mu\text{m}$  (proprietary undisclosed materials) silicate glass sample (also see Figures 4 and 8) was charged to  $-1100$  Volts by 10 keV electrons. The emission current was monitored by measuring the collection of electrons on the sensor field plate. By also knowing the capacitance of the sample ( $C_f = 35$  pF), the surface voltage decay due to the emission of charge onto the sensor field plate was calculated. After 18 minutes the measurement was discontinued, and started again after 38 minutes.**

Our experiments also show that "Malter" electron emission occurs for hours after turning off the electron beam. This Malter emission—similar to emission due to negative electron affinity in semiconductors—is a result of the prior radiation or optical excitations of valence electrons and their slow drift among traps towards the surface where they are subsequently emitted. Evidence for this comes from 10 keV-electron irradiation samples shown in Figure 9, where electrons are continually emitted for hours from the irradiated surface after the irradiation ceases. The long emission duration indicates that hopping is a dominant mechanism and that the conduction band is not significantly below the vacuum level. Additionally, monitoring current from the rear grounded electrode indicated that similar emission occurs at the rear electrode as well [4].

### Light-induced conductivity

Visible light has been used after charging the sample to investigate the conduction contributed by electrons (or holes) emitted from shallow trapping levels separately from the natural dark conductivity [4]. Kilovolt electron irradiations excited electrons into the conduction band, from where they decayed into traps. After irradiation, the trapped population was probed by exciting these trapped electrons into the conduction band to enhance conductivity so that the

sample surface voltage decayed. Light of frequency  $\nu$  can excite an electron transition from a trapped level into the conduction band provided that  $h\nu > \Delta E$ , where the trapped states are an energy  $\Delta E$  below the bottom of the conduction band. Thus, the relative currents for increasing light frequency provide information about the energy distribution of trapped states. In these experiments, a light source illuminated the pre-charged sample while a minimal positive battery voltage was maintained so that charge did not escape the surface of the sample. The light-induced conductivity caused the surface voltage to decay, and this voltage decay provided a sensitive monitor for conductivity.

In some samples, the effects of visible light-induced conductivity were found to be dominant while in other samples visible light provides negligible conductivity. A Teflon™ sample that was irradiated with an electron beam at 1 kV surface voltage showed almost no discharge. By contrast, polyimide samples 50  $\mu\text{m}$  thick that underwent similar irradiation were discharged in a few hours by a 1-watt incandescent filament. (A caution is evident from this result: the light emitted by an electron gun filament can potentially modify the charging process induced by the gun's electrons.) In some samples, light has been used to neutralize internal charging induced in prior tests so that further electron emission testing may proceed without initial charge in the sample [20,21].

### **Acknowledgments**

This work was supported by the NASA Space Environments and Effects (SEE) Program [7] and a USU Space Dynamics Laboratory Enabling Technologies Program Research Grant.

## References

1. Prasanna Swaminathan, A. R. Frederickson, J.R. Dennison, Alec Sim, Jerilyn Brunson, Eric Crapo, "Comparison Of Classical And Charge Storage Methods For Determining Conductivity Of Thin Film Insulators," Proceedings of the 8th Spacecraft Charging Technology Conference, October 20-24, 2003, Huntsville, Alabama.
2. W. Tillar Shugg, Handbook of Electrical and Electronic Insulating Materials, 2nd Ed; The Guide to Plastics by the Editors of Modern Plastics Encyclopedia, McGraw Hill, Inc., N.Y., 1970.
3. A.R. Frederickson, C. E. Benson and J. F. Bockman, "Measurement of Charge Storage and Leakage in Polyimides," Nuclear Instruments and Methods in Physics Research B, 454-60, 2003.
4. A.R. Frederickson and J. R. Dennison, "Measurement of Conductivity and Charge Storage in Insulators Related to Spacecraft Charging," accepted for publication in IEEE Trans. Nuc. Sci., Dec. 2003.
5. ASTM D 257-99, "Standard Test Methods for DC Resistance or Conductance of Insulating Materials" (American Society for Testing and Materials, 100 Barr Harbor drive, West Conshohocken, PA 19428, 1999).
6. IEC 93, International Electrotechnical Commission Publication 93, Methods of Test for Volume Resistivity and Surface Resistivity of Solid Electrical Insulating Materials, Second Edition, 1980.
7. J.R. Dennison and A.R. Frederickson, "Electronic properties of materials with application to spacecraft charging", NASA Space Environments and Effects (SEE) Program Grant NAS8-02031, 2002-2004.
8. A. Robb Frederickson and Donald H. Brautigam, "Mining CRRES IDM Pulse Data and CRRES Environmental Data to Improve Spacecraft Charging/Discharging Models and Guidelines," Final Report: NASA SEE Program Contract No. NAS7-1407, Task Order 10676, 2003; to be published.
9. Kapton polyimide film product information: Physical Properties, Report H-38492-1, (Dupont, Wilmington, DE, February, 1997); <http://www.dupontteijinfilms.com/> , June 20, 2002; The Red Book, RB 1, (Sheldahl Technical Materials, Northfield MN, 1995); <http://www.sheldahl.com/Product/TechMaterials.htm> , June 20, 2002.
10. Operators Manual, Model 341A, High Voltage Electrostatic Voltmeter, Trek, Inc., 11601 Maple Ridge Road, Medina, New York 14103, USA. Telephone: 1 (800) 367-8735 or 1 (585) 798-3140, <http://www.trekinc.com/> .



11. A.R. Frederickson, E.G. Mullen, K.J. Kerns and P.A. Robinson, "The CRRES IDM Spacecraft Experiment for Insulator Discharge Pulses," *IEEE Trans. Nuc. Phys.* 40(2), 233-241 (1993).
12. E. Mullen and M. Gussenhoven, "Results of Space Experiments: CRRES," in R.N. DeWitt, D. Duston, and A.K. Hyder (eds.) *The Behavior of Systems in the Space Environment*, pp. 605-654, (Kluwer Academic Publishers, 1993).
13. A.R. Frederickson, "Radiation Induced Electrical Current and Voltage in Dielectric Structures," AFCRL-TR-74-0582, 1974.
14. N. Nickles, R.E. Davies and J.R. Dennison, "Applications of SE Energy- and Angular-Distributions to Spacecraft Charging," *Proc. of 6<sup>th</sup> Spacecraft Charging Techno. Conf.*, (Hanscom Air Force Base, MA, 1999).
15. E.J. Sternglass, "Backscattering of Kilovolt Electrons from Solids," *Phys. Rev.* 95, 345-358 (1953); "An Experimental Investigation of Electron Back-scattering and Secondary Electron Emission From Solids, Ph.D. Dissertation, Cornell University, Ithica, NY, 1953.
16. A.J. Dekker, *Solid State Physics*, edited by Seitz and Turnbull (Academic Press, New York, 1958).
17. G.F. Dionne, "Origin of Secondary-electron-emission Yield-curve Parameters," *J. Appl. Phys.* 46 3347-3351 (1975); "Effects of Secondary Electron Scattering on Secondary Electron Emission," *J. Appl. Phys.* 44, 5361-5364 (1973).
18. J.E. Yates, A. Shih and Abrams, "Electron transport and emission properties of C(100)," *Phys. Rev. B*, 56, R4410-R4413 (1997).
19. R. Coelho, P Jestin, L. Levy and D. Sarrail, "On the Return-Voltage Buildup in Insulating Materials," *IEEE Trans. Elec. Insul.* 22, 683-90 (1987).
20. C.D. Thomson, V. Zavyalov, J.R. Dennison, Jodie Corbridge, "Electron Emission Properties of Insulator Materials Pertinent To The International Space Station," *Proceedings of the 8th Spacecraft Charging Technology Conference*, October 20-24, 2003, Huntsville, Alabama.
21. C.D. Thomson, Measurements of the Secondary Electron Emission Properties of Insulators, Ph.D. dissertation, Utah State University, 2004.
22. B. Gross and M. M. Perlman, *J. Appl. Phys.* 43, 853-7 (1972).